Large Eddy Simulation of Flashing Cryogenic Liquid with a Compressible Volume of Fluid Solver

Jan Wilhelm Gärtner*, Andreas Rees[2], Andreas Kronenburg[1], Joachim Sender[2], Michael Oschwald[2], Daniel Loureiro[1]
[1]Institut für Technische Verbrennung, Universität Stuttgart Herdweg 51 70174 Stuttgart Deutschland - Germany
[2]Institute of Space Propulsion, German Aerospace Center (DLR) Langer Grund 74239 Hardthausen - Germany
*Corresponding author: jan-wilhelm.gaertner@itv.uni-stuttgart.de

Abstract
For the development of new upper orbit thrusters with cryogenic propellants, it is important to understand the dynamics of oxidizer and fuel injection at near vacuum conditions before ignition. Due to the low ambient pressure with respect to the saturation pressure at the injection temperature, the propellants enter a superheated state and evaporate rapidly. This process is called flash evaporation. To simulate such a flashing cryogenic jet a compressible multiphase solver is developed in OpenFOAM. The homogeneous relaxation model (HRM) is chosen to model the phase change. For solving this multiphase problem, a one-fluid approach which solves for the mixture properties and phase fraction is selected. For the equation of state, the open source library CoolProp is used to calculate density, enthalpy and the saturation conditions. Further, the numerical methods to solve and capture the supersonic multiphase flow with a Volume of Fluid (VoF) method is described. The transition from mechanical break up to fully flashing spray and the change from subsonic to supersonic flow is investigated in detail. The numerical results are validated with experiments conducted at DLR Lampoldshausen which provide shadowgraph images. As a first approximation to fuel-oxidizer mixing, cryogenic nitrogen jet experiments at the DLR test bench M3.3 in Lampoldshausen are made and numerically investigated with large eddy simulations. It is noted that the flashing jet becomes supersonic and forms a shock shortly after the nozzle exit. This occurs despite the velocity being lower than the sonic velocities associated with each individual pure phase. The results show that the HRM model can predict the onset of the partial flashing flow, however fully flashing jet with 180 degree spray angle cannot be predicted with standard coefficients of the HRM model.

Keywords
flash-boiling, homogeneous relaxation model (HRM), compressible multiphase solver, flashing cryogenic nitrogen

Introduction

The current propellant for small in orbit thrusters of upper rocket stages and for reaction control of geostationary satellites is the hypergolic propellant hydrazine and its derivatives. This propellant has a high toxicity and flammability which requires complex and careful ground handling as well as loading procedures. In addition, it raises safety concerns for the rocket. The current space technological developments aims to replace these combustion systems with new, less harmful and operationally safer propellants. One potential alternative is the combustion of cryogenic oxygen with methane. To control the injection and ignition, the behavior of the fuels at high altitude conditions has to be understood. At these conditions, the fuels are injected prior to ignition into a near vacuum which leads to a supherheated state of the fuel and a rapid and strong evaporation. Due to the nearly instant evaporation of the liquid this process is called flash evaporation or flash boiling. The modeling and simulation of this physical process is a challenging task because of the complexity of the multiphase problem such as nucleation, bubble growth, coalescence and break up. To reduce the complexity and to enable the efficient computation of such multiphase problems one-equation models describing the phase change have been developed [1, 2]. Bilicki et al. [1] derived the homogeneous relaxation model (HRM) which relates the phase change to non-equilibrium of the vapor quality or mass fraction χ and a relaxation time θ. In the work of Zapolski et al. [2] an empirical description of the relaxation time is found, which is based on experiments known as "Moby Dick" [3].
Several authors have used the HRM model to simulate the flashing of liquids. Lee et al. [4] have used the HRM model to simulate the flashing of jet fuel in nozzles with a solver written in the object-oriented library OpenFOAM. Similarly, in the work of Schmidt et al. [5] the HRM model is used to simulate water discharge through short tubes and to compare the numerical results to experimental data. It has been found that the HRM model performed well without any model adjustments. Other authors have used the solver as a basis for the simulation of flash boiling in swirl injectors or the behavior of flashing cryogenic liquids through nozzles [6, 7]. The high pressure fit of the HRM model was used to simulate the flow of cryogenic liquid nitrogen through sharp-edged orifices, showing that the model can predict the mass flow rate accurately [8]. However, all these works focused on the simulation of the flow inside the pipe or nozzle and the immediate surroundings. Other work that focused on the flashing jet after the nozzle used an Euler-Lagrange approach with a predefined spray angle and defined droplet distribution [9, 10]. In this work no such assumption is made and an Euler-Euler approach is chosen to simulate the transition from the

liquid core to the dispersed droplet phase. The low and high pressure fits of the HRM model are used and compared to establish their suitability to predict the flashing flow after the exit from the nozzle into the low pressure domain.
Two families of numerical methods are common for simulating two phase flows. The first one uses a full set of momentum and energy equations for each phase and couples the interactions between both through the respective source terms. The second approach assumes that both phases form a locally homogeneous mixture which can be represented by one fluid. This means, that only one set of momentum and energy equations is solved and that the fluid properties are determined through an appropriate mixing rule. For this work the latter approach is chosen to reduce the computational effort needed to simulate a fully flashing jet. One assumption for this approach is a zero slip velocity between the two phases. Additionally it is assumed in this work that both phases share the same temperature.
With these assumptions the volume of fluid (VoF) solver compressiblePhaseChangeFoam is developed with the open source tool OpenFOAM. It is based on the standard solver compressibleInterFoam. The fluid properties are determined with the thermodynamic library CoolProp [11] before the simulation and are tabulated. During run time the required properties are looked up in the table and intermediate values are obtained through linear interpolation. This solver is then used to simulate fully flashing cryogenic nitrogen jets and the results are validated against experiments conducted at DLR Lampoldshausen. The experiments provide shadowgraph images to compare the spray angle to the numerical results.
The paper is organized as follows: First, the mathematical and numerical formulations for the mass, momentum, and energy equation are given together with a short overview of the HRM model. In the second part the computational setup and the experimental boundary conditions are described. Finally, the numerical results are compared with the experimental data.

Mathematical and numerical formulations
The mass, momentum, and energy equations are solved in a fully Eulerian framework. The liquid and vapor phases are solved together as one mixture assuming zero slip velocity and the same temperature for each phase. To describe the content of each phase in a cell the volume fraction $\alpha = V_\mathrm{l}/V_\mathrm{Cell}$ is used. For the mixture properties the set of governing equations then is:

Volume Fraction
$$\frac{\partial \rho_\mathrm{l}\alpha}{\partial t} + \nabla\cdot(\rho_\mathrm{l}\alpha\boldsymbol{u}) - \nabla\cdot\left(\frac{\rho_\mathrm{l}\nu_t}{\mathrm{Sc}_t}\nabla(\alpha)\right) = \dot{m}_\mathrm{l}, \tag{1}$$

Momentum
$$\frac{\partial \rho\boldsymbol{u}}{\partial t} + \nabla\cdot(\rho\boldsymbol{u}\boldsymbol{u}) = -\nabla p + \rho g + \nabla\cdot\boldsymbol{\tau}, \tag{2}$$

Energy
$$\frac{\partial \rho e}{\partial t} + \nabla\cdot(\rho e\boldsymbol{u}) = \frac{\partial p}{\partial t} - \nabla\cdot q + \nabla\cdot\left(\boldsymbol{u}\cdot\bar{\bar{\tau}}\right) + S_e, \tag{3}$$
$$\text{with } e = h + \frac{1}{2}\boldsymbol{u}^2,$$

where ρ, ρ_l, p, $\boldsymbol{u}$, ν_t, Sc_t, $\bar{\bar{\tau}}$, h, g are the mixture density, liquid density, pressure, mixture velocity vector, turbulent viscosity, turbulent Schmidt number, viscous stress tensor, mixture enthalpy and gravity respectively.
To solve the equation system a combined PISO, SIMPLE scheme, called PIMPLE is used in which first the volume fraction equation, the energy, and momentum equation is solved and then the velocity flux is corrected through a pressure equation which couples momentum with the mass conservation. As both phases are treated as compressible the volume fraction equations has to account for the changing densities. Using the linear model $\rho = \rho_0 + \psi p$ with the compressibility $\psi = \dfrac{\partial\rho}{\partial p}$ to calculate the density leads to,

$$\frac{\partial\alpha}{\partial t} + \frac{\alpha}{\rho_\mathrm{l}}\left(\psi_\mathrm{l}\frac{\mathrm{D}p}{\mathrm{D}t} + p\frac{\mathrm{D}\psi_\mathrm{l}}{\mathrm{D}t}\right) + \nabla\cdot(\alpha\boldsymbol{u}) - \nabla\cdot\left(\frac{\nu_t}{\mathrm{Sc}_t}\nabla(\alpha)\right) - \frac{\nu_t}{\mathrm{Sc_t}\rho_\mathrm{l}}(\nabla\alpha\cdot\nabla\rho_\mathrm{l}) = \frac{\dot{m}_\mathrm{l}}{\rho_\mathrm{l}}. \tag{4}$$

The last term on the LHS comes from the expansion of the diffusion term and is estimated to be small. This term is neglected in the following derivation. To include the information of the second phase in the equation, the compressibility term is replaced by adding Eq.(4) for the two phases and using that $\alpha_\mathrm{l} = 1 - \alpha_\mathrm{g}$. This gives,

$$\nabla\cdot\boldsymbol{u} + \frac{\psi_\mathrm{l}}{\rho_\mathrm{l}}\frac{\mathrm{D}p}{\mathrm{D}t} + \frac{p}{\rho_\mathrm{l}}\frac{\mathrm{D}\psi_\mathrm{l}}{\mathrm{D}t} = \alpha_\mathrm{g}\left(\frac{\psi_\mathrm{g}}{\rho_\mathrm{g}} - \frac{\psi_\mathrm{l}}{\rho_\mathrm{l}}\right)\frac{\mathrm{D}p}{\mathrm{D}t} - \alpha_\mathrm{g}\left(\frac{p}{\rho_\mathrm{g}}\frac{\mathrm{D}\psi_\mathrm{g}}{\mathrm{D}t} - \frac{p}{\rho_\mathrm{l}}\frac{\mathrm{D}\psi_\mathrm{l}}{\mathrm{D}t}\right) - \dot{m}_\mathrm{l}\frac{\rho_\mathrm{l}-\rho_\mathrm{g}}{\rho_\mathrm{l}\rho_\mathrm{g}}. \tag{5}$$

Inserting this into the Eq. (4) gives the final volume fraction equation,

$$\begin{aligned}\frac{\partial\alpha_\mathrm{l}}{\partial t} + \nabla\cdot(\alpha_\mathrm{l}\boldsymbol{u}) - \nabla\cdot\left(\frac{\mu_t}{\mathrm{Sc}_t}\nabla\alpha\right) =& \alpha_\mathrm{l}\left[\alpha_\mathrm{g}\left(\frac{\psi_\mathrm{g}}{\rho_\mathrm{g}} - \frac{\psi_\mathrm{l}}{\rho_\mathrm{l}}\right)\frac{\mathrm{D}p}{\mathrm{D}t}\right] + \alpha_\mathrm{l}\left[\alpha_\mathrm{g}\left(\frac{p}{\rho_\mathrm{g}}\frac{\mathrm{D}\psi_\mathrm{g}}{\mathrm{D}t} - \frac{p}{\rho_\mathrm{l}}\frac{\mathrm{D}\psi_\mathrm{l}}{\mathrm{D}t}\right)\right] \\ &+ \alpha_\mathrm{l}\nabla\cdot(\boldsymbol{u}) + \frac{\dot{m}_\mathrm{l}}{\rho_\mathrm{l}}\left(1 + \alpha_\mathrm{l}\left(\frac{\rho_\mathrm{l}-\rho_\mathrm{g}}{\rho_\mathrm{g}}\right)\right).\end{aligned} \tag{6}$$

Pressure Equation

For a general case, the total derivative of the density is derived in the work of Bilicki et al. [1] as a function of the mass fraction χ, pressure p, and enthalpy h (or temperature T),

$$\frac{\mathrm{D}\rho}{\mathrm{D}t} = \underbrace{\left(\frac{\partial\rho}{\partial\chi}\right)_{p,T}\frac{\mathrm{D}\chi}{\mathrm{D}t}}_{\text{Evaporation}} + \underbrace{\left(\frac{\partial\rho}{\partial p}\right)_{\chi,T}\frac{\mathrm{D}p}{\mathrm{D}t}}_{\text{Compressibility}} + \underbrace{\left(\frac{\partial\rho}{\partial T}\right)_{\chi,p}\frac{\mathrm{D}T}{\mathrm{D}t}}_{\text{Temperature}}. \tag{7}$$

The first term accounts for the effect of evaporation on the mixture density, the second considers the compressibility of the mixture density, and the last term modifies density due to changes in temperature.
Subtracting the mass conservation from Eq. (7) results in

$$-\rho\nabla\cdot\boldsymbol{u} = \left(\frac{\partial\rho}{\partial\chi}\right)_{p,T}\frac{\mathrm{D}\chi}{\mathrm{D}t} + \left(\frac{\partial\rho}{\partial p}\right)_{\chi,T}\frac{\mathrm{D}p}{\mathrm{D}t} + \left(\frac{\partial\rho}{\partial T}\right)_{\chi,p}\frac{\mathrm{D}T}{\mathrm{D}t}. \tag{8}$$

The default discretization of the momentum equation in OpenFOAM is,

$$\boldsymbol{u}_f = \left(\frac{H(\boldsymbol{u})}{a_p}\right)_f - \left(\frac{\nabla p}{a_p}\right)_f, \tag{9}$$

where a_p are the coefficients of the velocity matrix and $H(\boldsymbol{u})$ sums up the coefficients multiplied with their velocity of the neighboring cells as well as the unsteady part and all sources except the pressure gradient.
Taking Eq. (9), substituting it into Eq. (8) and dividing by the mixture density leads to

$$\nabla\cdot\left(\frac{\nabla p}{a_p}\right) - \nabla\cdot\left(\frac{H(\boldsymbol{u})}{a_p}\right) = \frac{1}{\rho}\left(\frac{\partial\rho}{\partial\chi}\right)_{p,T}\frac{\mathrm{D}\chi}{\mathrm{D}t} + \frac{1}{\rho}\left(\frac{\partial\rho}{\partial p}\right)_{\chi,T}\frac{\mathrm{D}p}{\mathrm{D}t} + \frac{1}{\rho}\left(\frac{\partial\rho}{\partial T}\right)_{\chi,p}\frac{\mathrm{D}T}{\mathrm{D}t}. \tag{10}$$

The material derivative of the mass fraction is represented analogous to the HRM model by,

$$\frac{\mathrm{D}\chi}{\mathrm{D}t} = \frac{\dot{m}_\mathrm{l}}{\rho}. \tag{11}$$

Describing the change of mass fraction with Eq. (11) and using the linear model from above gives the final pressure equation

$$\nabla\cdot\left(\frac{H(\boldsymbol{u})}{a_p}\right) - \nabla\cdot\left(\frac{\nabla p}{a_p}\right) + \frac{\rho_\mathrm{l}-\rho_\mathrm{g}}{\rho_\mathrm{g}}\frac{\dot{m}_\mathrm{l}}{\rho_\mathrm{l}} + \frac{\alpha_\mathrm{l}}{\rho_\mathrm{l}}\frac{\mathrm{D}\psi_\mathrm{l}p}{\mathrm{D}t} + \frac{\alpha_\mathrm{g}}{\rho_\mathrm{g}}\frac{\mathrm{D}\psi_\mathrm{g}p}{\mathrm{D}t} = 0. \tag{12}$$

Energy Equation

Starting from the energy eqation (3) the conservation of energy can be expressed for the two phases through temperature as:

$$\text{Liquid} \qquad \alpha_\mathrm{l}\rho\frac{\mathrm{D}T}{\mathrm{D}t} + \frac{\alpha_\mathrm{l}}{c_{p,\mathrm{l}}}\rho\frac{\mathrm{D}K}{\mathrm{D}t} = \left(\frac{\partial p}{\partial t} + \nabla\cdot(k_\mathrm{l}\nabla T)\right)\frac{\alpha_\mathrm{l}}{c_{p,\mathrm{l}}} + \frac{\alpha_\mathrm{l}}{c_{p,\mathrm{l}}}\dot{m}_\mathrm{l}h_\mathrm{g} - \frac{\rho}{\rho_\mathrm{l}c_{p,\mathrm{l}}}\dot{m}_\mathrm{l}h_\mathrm{l} \tag{13}$$

$$\text{Vapor} \qquad \alpha_\mathrm{g}\rho\frac{\mathrm{D}T}{\mathrm{D}t} + \frac{\alpha_\mathrm{g}}{c_{p,\mathrm{g}}}\rho\frac{\mathrm{D}K}{\mathrm{D}t} = \left(\frac{\partial p}{\partial t} + \nabla\cdot(k_\mathrm{g}\nabla T)\right)\frac{\alpha_\mathrm{g}}{c_{p,\mathrm{g}}} - \frac{\alpha_\mathrm{g}}{c_{p,\mathrm{g}}}\dot{m}_\mathrm{g}h_\mathrm{g} \tag{14}$$

Here, it is assumed that both phases share the same temperature and that the energy for the phase change is drawn from the two phases mass fraction,

$$S_{e,\mathrm{l}} = -S_{e,G} = \frac{\alpha_\mathrm{l}\rho_\mathrm{l}}{\rho}\dot{m}_\mathrm{l}h_\mathrm{g}. \tag{15}$$

Combining equations Eq. (13) and Eq. (14) gives the final energy equation,

$$\begin{aligned}\rho\frac{\mathrm{D}T}{\mathrm{D}t} + \left(\frac{\alpha_\mathrm{l}}{c_{p,\mathrm{l}}} + \frac{\alpha_\mathrm{g}}{c_{p,\mathrm{g}}}\right)\left(\rho\frac{\mathrm{D}K}{\mathrm{D}t} - \frac{\partial p}{\partial t}\right) - (\alpha_\mathrm{l}\nabla\cdot(\alpha_{\mathrm{Eff},\mathrm{l}}\nabla T) + \alpha_\mathrm{g}\nabla\cdot(\alpha_{\mathrm{Eff},\mathrm{g}}\nabla T)) = \\ \dot{m}_\mathrm{l}h_\mathrm{g}\left(\frac{\alpha_\mathrm{l}}{c_{p,\mathrm{l}}} + \frac{\alpha_\mathrm{g}}{c_{p,\mathrm{g}}}\right) - \frac{\rho}{\rho_\mathrm{l}c_{p,\mathrm{l}}}\dot{m}_\mathrm{l}h_\mathrm{l},\end{aligned} \tag{16}$$

with α_Eff as the turbulent thermal diffusivity defined as $\alpha_\mathrm{Eff} = \frac{k}{c_p} + \frac{k_t}{c_p}$.

HRM Model

The mass transfer is modeled with the homogeneous relaxation model (HRM) which has been originally developed by Downar-Zapolski et al. [2] and is fitted to experiments for flashing water. The HRM model describes the change of mass fraction χ as being proportional to the difference to equilibrium conditions and the rate change is expressed by a relaxation time Θ. In this work the equation of Downar-Zapolski et al. [2] is changed so that the mass fraction is based on the liquid mass and not on the vapor mass. With this change the equilibrium mass fraction is,

$$\overline{\chi} = \frac{h - h_{\mathrm{SG}}(p)}{h_{\mathrm{SL}}(p) - h_{\mathrm{SG}}(p)}. \tag{17}$$

where h is the mixture enthalpy $h = \chi h_{\mathrm{l}}(p,T) + (1-\chi)h_{\mathrm{SG}}(p)$, $h_{\mathrm{SL}}(p)$ the saturation enthalpy of the liquid and $h_{\mathrm{SG}}(p)$ the saturation enthalpy of the vapor for the given pressure p. Using this definition of the mass fraction the homogeneous relaxation model is given by

$$\frac{\mathrm{D}\chi}{\mathrm{D}t} = -\chi \frac{h_{\mathrm{l}}(p,T) - h_{\mathrm{SL}}(p)}{h_{\mathrm{SG}}(p) - h_{\mathrm{SL}}(p)} \frac{1}{\Theta}. \tag{18}$$

The relaxation time Θ is based on the experimental data from Reocreux (1974), known as the "Moby Dick" experiments. With this data, two formulation of the relaxation time based on the void fraction and the pressure is found [2], a high pressure and low pressure fit. The relaxation time for the low pressure fit is described by,

$$\Theta = \Theta_0 \epsilon^{-0.257} \psi^{-2.24}. \tag{19}$$

Here, $\Theta_0 = 6.51 \times 10^{-4}$ s and has the dimensions of time in seconds. The void fraction ϵ and the non-dimensional pressure difference ψ are defined by,

$$\epsilon = \frac{\rho_l - \rho}{\rho_l - \rho_v}, \tag{20}$$

$$\psi = \frac{p_s(T) - p}{p_s(T)}, \tag{21}$$

respectively. The high pressure fit uses different empirically fitted exponential values and a different equation to calculate the pressure ratio ψ,

$$\Theta = \Theta_0 \epsilon^{-0.54} \psi^{-1.76}, \tag{22}$$

$$\psi = \frac{p_s(T) - p}{p_c - p_s(T)}, \tag{23}$$

where $\Theta_0 = 3.84 \times 10^{-7}$ s and p_c is the critical pressure.

Simulation Setup and Experimental Data

The experiments for the validation are conducted at DLR Lampoldshausen where cryogenic liquid nitrogen is injected into a controllable low pressure environment. To describe the strength of a flashing flow, superheat R_p typically is used, which relates the saturation pressure at the given temperature to the ambient pressure [12],

$$R_p = \frac{p_{\mathrm{sat}}}{p_\infty}. \tag{24}$$

The experimental investigations provide three different nitrogen sprays with varying superheat ratios, starting from a low superheat $R_p = 2.4$ to a fully flashing flow with $R_p = 49.1$. For the inflow a short nozzle with an L/D ratio of 2.2 is used. The shadowgraph images of the three sprays are shown in Figure 1. Table 1 shows the boundary conditions of the experiment.

The simulation domain consists of a cylinder with a radius of 25 mm and a height of 80 mm which covers the visible part of the experimental chamber. For cases 2 and 3 a mesh size of 10.9 million cells is used and for case 1 an

Table 1. Experimental boundary conditions

Case	Superheat	Chamber Pressure [bar]	Injection Temperature [K]	Velocity [m/s]	Injection pressure [bar]
1	49.1	0.07	89.7	13.9	4.71
2	4.7	0.74	89.6	7.2	3.94
3	2.4	1.45	89.7	7.0	3.98

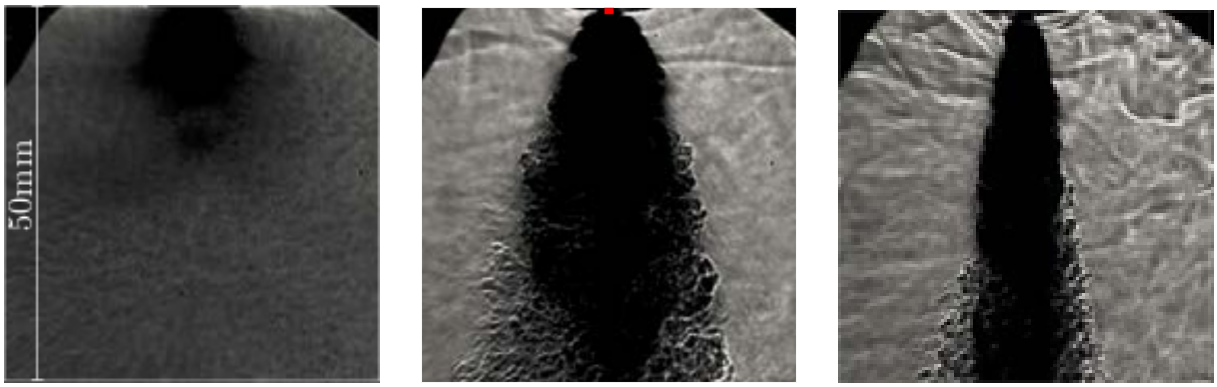

(a) Case 1: $R_p = 49.1$ (b) Case 2: $R_p = 4.7$ (c) Case 3: $R_p = 2.4$

Figure 1. Shadowgraph images of the nitrogen spray for different superheat ratios R_p. The nozzle outlet is marked with a red square for case 2.

increased mesh resolution with 22 million cells is needed. In all cases a structured mesh is used with a cell grading at the inlet of 3.3 and a cell length of 75 µm at the inlet. The mesh for case 1 is refined in the radial direction compared to case 2 and case 3. The time is discretized with the Crank-Nicolson time scheme using a blending factor of 0.9 towards the first order Euler scheme. All divergence schemes use total variation diminishing such as the van Leer scheme for the volume fraction and the limited linear scheme for all other terms. This is required to avoid numerical instabilities at large gradients present at shocks. The unresolved turbulence of the LES simulation is modeled with the Smagorinsky-Lilly Model. Surface compression terms in the volume fraction equation are switched off, as a liquid vapor interface is not resolved. At the outlet the boundary condition for pressure is set to a fixed value and all other boundary conditions use zero gradient. The patch next to the inlet uses as well zero gradient boundary conditions except for the velocity where a no slip condition is set to account for the wall of the nozzle.
From the experimental results it is assumed that nearly pure liquid flows out of the nozzle into the vacuum chamber. With this assumption for the fluid properties, the inlet profile is generated with an in-house code called pipeFoam which uses a hybrid LES-RANS approach (Spalart-Allmaras IDDES) to simulate the flow in the nozzle leading up to the experimental chamber to get a correct time transient inflow velocity profile.
The operating conditions of case 1 are below the pressure of the triple point $p_{triple} = 12\,519.8$ Pa and as a consequence enthalpy values at the saturation line based on pressure cannot be computed. For the calculation of the source term in the HRM model the values are then limited to the minimum value of the saturation line.

Results and discussion

The three experimental test cases presented in Figure 1 are simulated with the newly developed compressiblePhaseChangeFoam solver. To compare the numerical results with the shadow graph images of the experiments, the Laplacian of the density is calculated and then integrated along the x direction which is perpendicular to the z-y plane shown in Figure 2 [13]. To compare the results with the camera image, the contrast is adjusted for one case to match the experimental image and then kept constant for the other cases. Further, a square root function is applied to the normalized data set to enhance the contrast of low value regions. As the Laplacian of the mixture density cannot account for the light refraction of the subgrid droplets or bubbles, the integrated volume fraction is shown as well in Figure 3 using a linear relationship for the gray scale. Comparing the numerically generated shadowgraph images to the integrated volume fraction shows good agreement and suggests that using the Laplacian of the mixture density is feasible.
At first the low pressure fit of the HRM model is used. Additionally, the volume fraction diffusion is switched off to reduce simulation times. Comparison with simulations where it is included showed no difference in the results. The reason for this is that the spray breaks up soon after exiting the nozzle which leads to a more uniform distributed volume fraction field. This results in low gradients giving to insignificant contribution for the diffusion term.
Figure 2 shows the results for the three cases using the low pressure coefficients of Eq. (19). The experimental result for case 2 shows an immediate spreading of the jet after the nozzle exit to about 2.5 times the nozzle diameter. In contrast the computations with the low pressure fit predicts no direct spreading of the jet at the nozzle exit.
Case 1 with a fully flashing flow is also showing a significantly smaller spray angle than can be observed in the shadow graph image. Additionally, a shock is visible about 8 diameters downstream of the nozzle exit which is embedded within the two phase flow and therefore not visible with the shadowgraph method [12].
In a second step the cases 1 and 2 are simulated using the high pressure fit for the HRM model. Here, the results are shown with the volume fraction diffusion term included. Figure 4 shows that the spreading angle is larger than for the low pressure fit and the initial jet spreading after the nozzle exit is now in agreement with the experimental result for case 2. However, a further spreading of the jet downstream is not observed but present for the epxerimental data. This indicates, that the HRM model cannot capture the effects of the droplet evaporation after the spray break up correctly. The velocity plot in Figure 4b shows that initially a 180 degree spray angle is seen at the nozzle, yet it does not expand over the complete domain. A possible explanation is, that the equation of the HRM model

is not well defined for regions below the triple point where saturation conditions based on the pressure can no longer be computed. Another explanation is that the HRM model may be well suited for regions where the spray is dense, i.e. a continuous liquid phase exist with dispersed bubbles inside. However, after the jet disintegration when hot droplets continue to evaporate the approximations implied by the HRM model no longer hold. Further, direct coupling of droplet evaporation and turbulence could be of importance and are currently not directly modeled.
The shock observed in the numerical results is in agreement with experimental results of Lamanna et al. [12] who have investigated the shock structure of retrograde and non-retrograde fluids. They concluded, that fluids with a low reduced temperature (T/T_c) will show the shock structure for flashing flows which is also the case for the cryogenic nitrogen in case 1. It is also stated that the shock is not visible with a shadowgraph method for fluids with a higher enthalpy of vaporisation which explains that the shock structure is hidden in the experimental shadowgraph image.

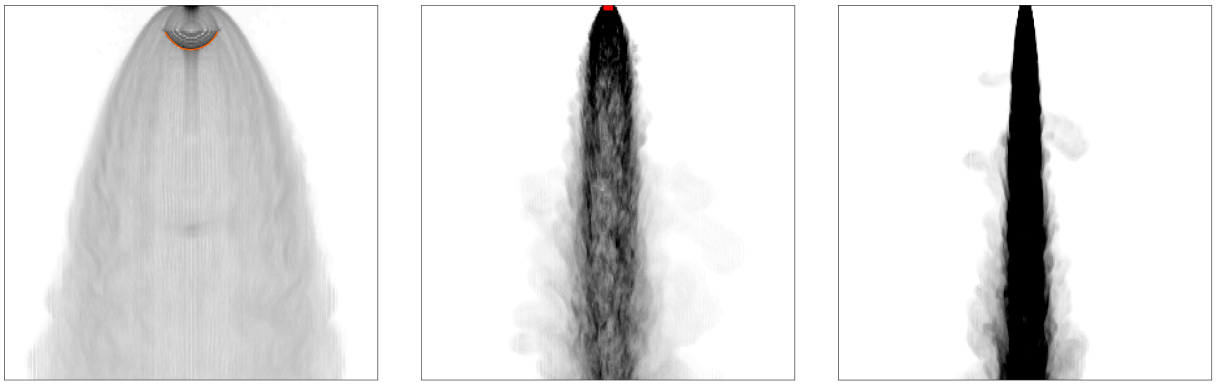

(a) Case 1: $R_p = 49.1$ (b) Case 2: $R_p = 4.7$ (c) Case 3: $R_p = 2.4$

Figure 2. Numerical grey scale image of the integrated Laplacian of the mixture density using the low pressure fit of the HRM model. In case 2 the nozzle diameter is marked with a red square. The shock position in case 1 is marked in orange.

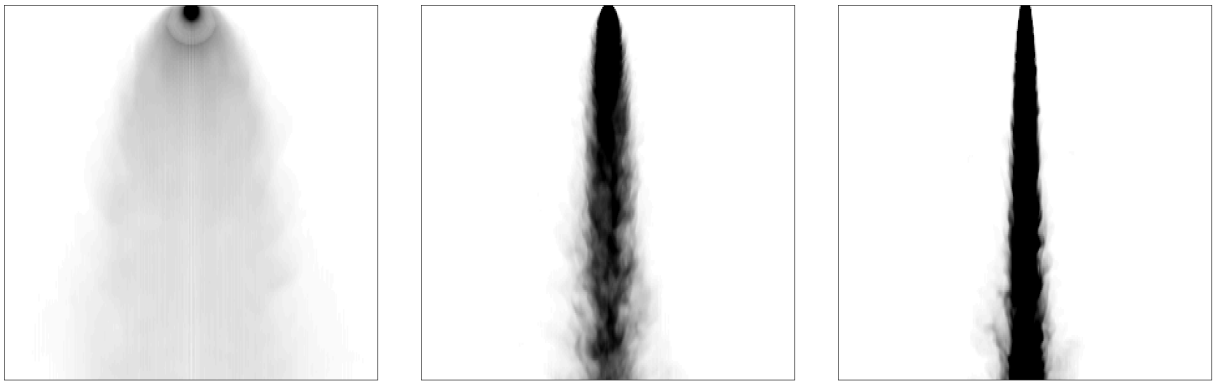

(a) Case 1: $R_p = 49.1$ (b) Case 2: $R_p = 4.7$ (c) Case 3: $R_p = 2.4$

Figure 3. Normalized integrated volume fraction with the low pressure fit of the HRM model.

Conclusions

The results show, that the HRM model with the high pressure fit can predict the spray angle for the partial flashing flow after the nozzle exit. Similar, a 180 degree spreading is seen directly after the nozzle exit but does not expand throughout the complete domain for the fully flashing case. The developed compressible volume of fluid solver can resolve the shock front present for the fully flashing flow in case 1. The absence of the shock in the shadowgraph images can be explained by the high enthalpy of vaporisation that hides it within the flow [12]. The jet spray break up in the cases 2 and 3 with a low superheat value is not predicted correctly by the developed solver.
For future work an additional transport equation for the surface density can be included. With this additional scalar information the mean droplet size is available and can be used in the phase change term to model the evaporation of hot droplets directly and restrict the HRM model to the part before the disintegration into droplets. To include the subgrid effects of droplet evaporation and vapor interaction a PDF method as described by Navarro-Martinez [14] can be used. In addition experimental velocity data sets obtained through PDA measurement as well as an improved shadowgraph set-up can be used to further validate the numerical results and to get a quantitative comparison.

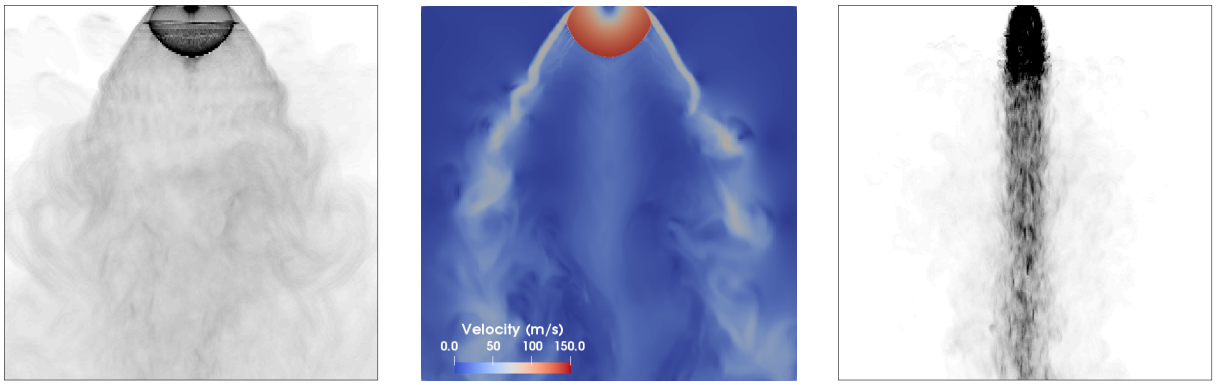

(a) Case 1: $R_p = 49.1$ (b) Case 1: Velocity profile (c) Case 2: $R_p = 4.7$

Figure 4. Numerical grey scale image of the integrated Laplacian of the mixture density using the high pressure fit of the HRM model and velocity magnitude of case 1.

Acknowledgements
The authors thank the German Research Foundation (DFG) for financial support of the project within the collaborative research center SFB-TRR 75. The authors also thank for the access to the supercomputer ForHLR funded by the Ministry of Science, Research and the Arts Baden-Württemberg and by the Federal Ministry of Education and Research. Further, D. Loureiros work is part of the HAoS-ITN project and has received funding from the European Union's Horizon 2020 research and innovation program under the Marie Skłodowska-Curie grant agreement No 675676.

Nomenclature

α	volume fraction [-]
ϵ	void fraction [-]
g	gravitation $[m/s^2]$
h	specific enthalpy $[m^2/s^2]$
k	thermal conductivity $[W/(mK)]$
K	kinetic energy $[m^2/s^2]$
m	mass $[kg]$
ν_t	turbulent kinematic viscosity $[m^2/s]$
p	pressure $[Pa]$
p_{sat}	saturation pressure $[Pa]$
ψ	compressibility $[s^2/m^2]$
ρ	density $[kg/m^3]$
R_p	superheat ratio [-]
Sc_t	turbulent Schmidt number
Θ	relaxation time [s]
χ	mass fraction [-]

References

[1] Bilicki, Z., and Kestin, J., 1990. "Physical aspects of the relaxation model in two-phase flow". *Proceedings of the Royal Society of London A: Mathematical, Physical and Engineering Sciences, 428*(1875), pp. 379–397.
[2] Downar-Zapolski, P., Bilicki, Z., Bolle, L., and Franco, J., 1996. "The non-equilibrium relaxation model for one-dimensional flashing liquid flow". *International Journal of Multiphase Flow, 22*(3), pp. 473 – 483.
[3] Bouré, J., Fritte, A., Giot, M., and Réocreux, M., 1976. "Highlights of two-phase critical flow: On the links between maximum flow rates, sonic velocities, propagation and transfer phenomena in single and two-phase flows". *International Journal of Multiphase Flow, 3*(1), pp. 1 – 22.
[4] Lee, J., Madabhushi, R., Fotache, C., Gopalakrishnan, S., and Schmidt, D., 2009. "Flashing flow of superheated jet fuel". In Proceedings of The Combustion Institute, Vol. 32, pp. 3215–3222.
[5] Schmidt, D., Gopalakrishnan, S., and Jasak, H., 2010. "Multidimensional simulation of thermal non-equilibrium channel flow". *International Journal of Multiphase Flow, 36*, 04, pp. 284–292.
[6] Neroorkar, K., Gopalakrishnan, S., R. O. Grover, J., and Schmidt, D., 2011. "Simulation of flash boiling in pressure swirl injectors". pp. 179–188.
[7] Lyras, K., Dembele, S., Schmidt, D. P., and Wen, J. X., 2018. "Numerical simulation of subcooled and superheated jets under thermodynamic non-equilibrium". *International Journal of Multiphase Flow, 102*, pp. 16–28.

[8] Lyras, K., Dembele, S., Vyazmina, E., Jallais, S., and Wen, J., 2017. "Numerical simulation of flash-boiling through sharp-edged orifices". *International Journal of Computational Methods and Experimental Measurements, 6*, 10, pp. 176–185.

[9] Ramcke, T., Lampmann, A., and Pfitzner, M., 2017. "Simulations of injection of liquid oxygen/gaseous methane under flashing conditions". *Journal of Propulsion and Power, 34*(2), pp. 395–407.

[10] Rachakonda, S. K., Wang, Y., and Schmidt, D. P., 2018. "Flash-boiling initialization for spray simulations based on parametric studies". *Atomization and Sprays, 28*(2).

[11] Bell, I. H., Wronski, J., Quoilin, S., and Lemort, V., 2014. "Pure and pseudo-pure fluid thermophysical property evaluation and the open-source thermophysical property library coolprop". *Industrial & Engineering Chemistry Research, 53*(6), pp. 2498–2508.

[12] Lamanna, G., Kamoun, H., Weigand, B., and Steelant, J., 2014. "Towards a unified treatment of fully flashing sprays". *International Journal of Multiphase Flow, 58*, pp. 168 – 184.

[13] Panigrahi, P. K., and Muralidhar, K., 2012. "Laser schlieren and shadowgraph". In *Schlieren and Shadowgraph Methods in Heat and Mass Transfer*. Springer, pp. 23–46.

[14] Navarro-Martinez, S., 2014. "Large eddy simulation of spray atomization with a probability density function method". *International Journal of Multiphase Flow, 63*, pp. 11 – 22.